Research Article | Vol. 3, No. 12 / 15 December 2020 / OSA Continuum 3324

Experimental demonstration of the near-quantum optimal receiver

M. V. JABIR,[1] I. A. BURENKOV,[1,2] N. FAJAR R. ANNAFIANTO,[1] A. BATTOU,[1] AND S. V. POLYAKOV[1,3,*]

[1]National Institute of Standards and Technology, Gaithersburg, MD 20899, USA
[2]Joint Quantum Institute & University of Maryland, College Park, MD 20742, USA
[3]Department of Physics, University of Maryland, College Park, MD 20742, USA
[*]spoly@nist.gov

Abstract: We implement the cyclic quantum receiver based on the theoretical proposal of Roy Bondurant and demonstrate experimentally below the shot-noise limit (SNL) discrimination of quadrature phase-shift keying signals (PSK). We also experimentally test the receiver generalized for longer communication alphabet lengths and coherent frequency shift keying (CFSK) encoding. Using off-the-shelf components, we obtain state discrimination error rates that are 3 dB and 4.6 dB below the SNLs of ideal classical receivers for quadrature PSK and CFSK encodings, respectively. The receiver unconditionally surpasses the SNL for M=8 PSK and CFSK. This receiver can be used for the simple and robust practical implementation of quantum-enhanced optical communication.

© 2020 Optical Society of America under the terms of the OSA Open Access Publishing Agreement

1. Introduction

In digital communication, information is encoded into a finite set of physical states at a transmitter, sent through a communication channel and measured (discriminated) at a receiver [1,2]. Today, optical pulses are the preferred information carriers for long-distance communication [3,4]. The global volume of data exchange has reached 200 exabytes per month and continues to rise exponentially [5]. The exponential growth in data leads to "capacity crunch" in the underlying physical systems. One of the possible methods to deter the exponential growth of physical resources for communication is to use quantum, rather than classical measurement at the receiver. By doing so, the optical energy required to transmit bits of information with the same reliability can be reduced, when compared to traditional receivers. On the other hand, implementation of quantum measurement may be difficult, hindering its practical use. Here we experimentally show the receiver that could solve this lingering issue.

Coherent states of light are excellent for optical communication because they are easy to generate, modulate, and detect even in the presence of channel losses. Digital information can be encoded in frequency, phase and/or amplitude of coherent states. Encoding methods differ in their use of these parameters. The number of coherent states that comprise the communication alphabet can also differ. The encoding method and the alphabet length are selected to optimize data transfer given the practical limitations of the communication channel. There are, however, fundamental limits on such optimization. Measurement noise at the receiver limits the data transfer even in otherwise noiseless optical channels. Classical optical receivers are typically limited by the shot noise [6,7] that gives rise to a classical minimal error probability for the discrimination. However, from a quantum standpoint, lower error probabilities can be achieved. This quantum limit is known as the Helstrom bound (HB) [8]. The Dolinar receiver [9] theoretically can reach HB for discrimination of two coherent states. Unless a quantum computer is used [10], no quantum measurement reaches the HB for longer alphabets. Yet, practical state discrimination below the SNL is still possible: quantum-measurement enhanced receivers with variety of discrimination strategies were investigated in a number of experimental and theoretical studies [9,11–26]. In

#409200
Journal © 2020
https://doi.org/10.1364/OSAC.409200
Received 4 Sep 2020; accepted 5 Nov 2020; published 19 Nov 2020

OSA CONTINUUM

many prior experiments, [20,21,27–29] discrimination error rates below the classical shot noise limit (SNL) were demonstrated.

To date, most of the experimental research is focused on quantum receivers with an adaptive optical state displacement of the input followed by a single-photon detector (SPD). The most accurate updating strategy to date is based on Bayesian inference using measured photon detection times [19,23,29]. However, the Bayesian likelihood depends on the input intensity, modulation scheme, and other experimental conditions and requires excessive real-time calculations at the receiver. To our knowledge, no experiment reached the below-SNL discrimination of M>4 PSK alphabets, regardless of the multiple efforts to improve state discrimination for quadrature ($M = 4$) phase-shift keying (QPSK) [17,19–21,25,26,30]. Surprisingly, a much simpler strategy exists. In 1993 Roy S. Bondurant theoretically described a "near-quantum optimal receiver" with a sequential probing strategy for QPSK [12]. Specifically, he found analytically the expression for state discrimination error probability, that is going below the SNL and has the same asymptotic behavior as the QPSK HB in the limit of large input signal energies. With a slight modification to Bondurant scheme, where the sequential probing strategy is looped into a cycle the generalized receiver can be made versatile. Because of its simplicity, the probing strategy works for any experimental conditions, any encoding type, and any alphabet length, in contrast to previous strategies. However, until now, the Bondurant receiver that unconditionally outperforms the SNL has not been experimentally realized.

Here we experimentally implement this versatile, scalable receiver. We demonstrate below the absolute SNL discrimination error rates for a long PSK alphabet ($M = 8$) for the first time (Note: here and further in the manuscript we refer to the homodyne-SNL of an ideal classical receiver with unit efficiency if not specified otherwise). We experimentally show that the cyclic receiver can discriminate optical states below the SNL error rate for a range of different modulation protocols, namely CFSK [23] and PSK. We demonstrate that the error rate of the communication link at a given input energy can be improved by optimizing the modulation protocol, and not the receiver. This simple receiver strategy could be particularly advantageous for energy-efficient practical telecommunication links.

2. Generalized Bondurant receiver

Consider an alphabet of M coherent states, $|\alpha_i\rangle$, where $i \in 1 \cdots M$. An adaptive measurement in a Bondurant receiver is comprised of a quantum displacement operation on an unbalanced beam splitter followed by SPD, shaded rectangle in Fig. 1. The Bondurant receiver uses photon detection times for the feedback by switching the probing hypothesis sequentially immediately after each photon detection ($\alpha_1 \rightarrow \alpha_2 \rightarrow \cdots \rightarrow \alpha_M$). The probability of an SPD to produce a click is high when the probing state is different from the input state. Ideally, when the hypothesis matches the correct input state, quantum displacement fully extinguishes the input, so that no photons can be detected. In the original theoretical proposal [12] two types of QPSK receivers are analyzed. The type 1 receiver returns the hypothesis at the end of each input pulse as the discrimination result. Therefore, with an ideal state displacement and in the absence of dark counts at the detector, the detection of $M - 1$ photons is required to cycle between all the hypotheses and discriminate the input state with certainty. For QPSK $M - 1 = 3$ photons required. Clearly, most errors occur at low input energies, i.e. when the detection of 3 photons cannot be guaranteed. The type 2 QPSK receiver also probes hypotheses sequentially, but in addition, it uses photon interarrival times to improve accuracy when only 2 photons were detected.

In a practical setting, neither the perfect displacement of the input state to vacuum nor the dark-count-free single-photon detection are possible. Therefore, the detector in Fig. 1 can fire even if the hypothesis is correct. A simple modification of the Bondurant's sequential hypothesis switching with a cyclic switching, i.e. $\alpha_1 \rightarrow \alpha_2 \rightarrow \cdots \rightarrow \alpha_M \longrightarrow \alpha_1 \rightarrow \cdots$, ensures that the receiver will not be thrown off by an occasional background or dark photodetection. This simple

OSA CONTINUUM

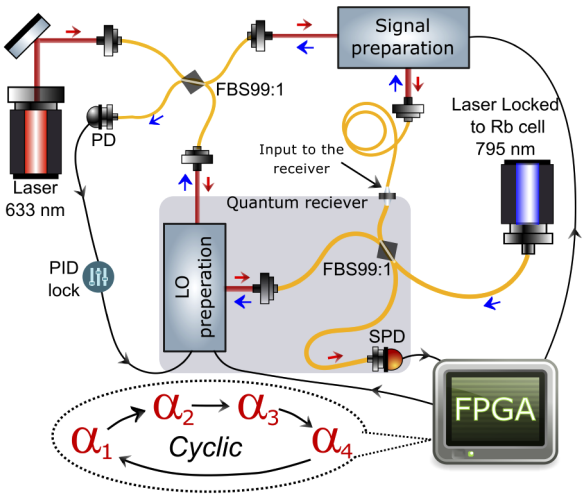

Fig. 1. The Bondurant receiver testbed. The input signal and the LO are prepared from 633 nm laser light using acousto-optic modulators (AOM)s in a double pass configuration (not shown). The receiver is comprised of a LO, 99:1 FBS and an SPD. The electronic output of the SPD is connected to the FPGA that implements the cyclic discrimination strategy. The same FPGA generates the RF signal for AOMs. A second laser locked to a rubidium atomic line at 795 nm is used to lock the setup interferometrically. The interferometric feedback is generated by a photodiode (PD). Red and blue arrows show the direction of 633 nm and 795 nm respectively.

modification generalizes the type 1 Bondurant receiver for the use with any alphabet length and any encoding. We implement this receiver experimentally.

The experimental setup of the receiver is shown in Fig. 1. The continuous-wave laser at 633 nm is attenuated and sent via fiber to a 99:1 fiber beam splitter (FBS) to generate the local oscillator (LO) and the signal pulse, respectively. Both the states are prepared with acousto-optic modulators (AOM)s in double-pass configuration [31]. After the state preparation, both the LO and the signal pulse are coupled back into fiber and sent onto a quantum receiver. The adaptive receiver is built with a 99:1 fiber beam splitter for state displacement and a commercial SPD [32]. The field-programmable gate array (FPGA) generates the radio-frequency (RF) inputs for AOMs, and uses electric pulses produced by the SPD to execute the cyclic state discrimination strategy in real-time. We point out that due to simplicity of this receiver, a fast, power-efficient counter register can be used. The Mach-Zehnder interferometer formed by the pair of 99:1 FBSs in Fig. 1 is stabilized using back-propagating 795 nm light and a mirror with piezoelectric actuator controlled by stand-alone locking electronics. The lock is set at the minimum of the 633 nm fringe so that the LO displaces the input signal to vacuum if both states are identical. The 795 nm laser is frequency stabilized to a rubidium atomic line. The signal and the LO preparation stages generate identical coherent states during the lock cycle of the Mach-Zehnder interferometer. The stabilization laser is switched off while the FPGA executes the discrimination algorithm. The duty factor of signal pulses is 50%.

To find the system efficiency of our receiver we measured optical transmission loss in the optical components to be 11.4(5)% and detection efficiency of the SPD of 84.0(3)%. Thus the system efficiency is 74.5(6)%. The symbol duration is $T = 32.7\ \mu s$ results in the bit rate of 30580 bits/s and 45871 bits/s for alphabet lengths $M = 4$ and 8 respectively. The measured visibility of the interferometer is 99.7%. Note that, even though the theoretical discrimination error rate was estimated for a balanced displacement, we have used the optimal displacement, c.f. [19,24].

OSA CONTINUUM

3. Experimental results

3.1. Phase shift keying

We tested the Bondurant receiver for $M = 4$ and 8 PSK encodings. PSK encodes information in M coherent states that differ by phase: $\alpha_i(\omega, \theta) = \alpha(\omega, (i-1)2\pi/M)$, $i \in 1..M$. The PSK constellation diagram is shown in Fig. 2(a,b). We experimentally measure the state discrimination error rate for the input states with different energies, Fig. 2(c,d). To best compare energies of input coherent states for the alphabets with different lengths, we present the input optical energy as the average number of photons per bit. We compare our experimental results with the Bondurant's theoretical prediction scaled for our system detection efficiency. The measured error rate is lower than the theoretical prediction for input energies corresponding to up to 1 photon per bit because LO with the optimized average number of photons is used for discrimination of signals with a very low average number of signal photons. However, the error rate saturates for higher input energies due to imperfect interferometric visibility and finite switching time of the AOM. Note that the receiver exhibits lower than classically achievable SNL in the range of 1 to 3.5 photons per bit. The best nonclassical performance of this receiver occurs at 2.3 photons per bit, where our error rate is nearly 3 dB lower than the SNL, (inset of Fig. 2(c)). We tested our implementation of the receiver for a longer alphabet $M = 8$ and compared our experimental results with the SNL, see Fig. 2(d). We observe that the measured error rate is below the SNL by 0.2 dB at ≈ 3.5 photons per bit. To quantify the degree of quantum measurement advantage of the Bondurant receiver over a classical measurement, we also compare the measured error rates with the SNL adjusted to the system efficiency of our receiver, dashed line in Fig. 2. We observe that our receiver significantly outperforms a classical receiver with the same system efficiency: the error rate is nearly 6 dB lower for $M = 4$ and 3 dB lower for $M = 8$.

3.2. Coherent frequency shift keying

Since the cyclic strategy works with any encoding, we tested the Bondurant receiver for a different encoding scheme. The CFSK uses M phase-synchronized coherent states that differ in phases and frequencies such that detunings and initial phases between the adjacent states are equal, $\alpha_i(\omega, \theta) = \alpha(\omega_0 + (i-1)\Delta\omega, (i-1)\Delta\theta)$, $i \in 1..M$ [23]. The CFSK constellation diagram is shown in Fig. 3(a) and (b). The unique feature of CFSK is that it can be optimized for minimal input energy requirements based on the properties of the measurement method, here a displacement based on a cyclic strategy. Figure 3(c) and (d) show the optimization map of CFSK parameters given the input signal energy of one photon per bit for $M = 4$ and $M = 8$, respectively. Surprisingly, these maps are different from the optimization maps for Bayesian receivers, c.f. [23]. We have used the value of $\Delta\omega T = \pi/2$, where $\Delta\omega$ is $2\pi\times$7629Hz, and $\Delta\theta = 0.36\pi$ and 0.15π for $M = 4$ and $M = 8$ alphabets respectively, green dots in the map shows the values used in the experiment.

Figure 4 shows the experimentally measured error probability for input states with different energies. In comparing experimental results with the SNL (red solid line in Fig. 4), we demonstrate that our implementation of the cyclic receiver has a lower discrimination error than allowed by the SNL in the range of 0.5 to 3 photons per bit for $M = 4$ CFSK and in the range of 1.3 to 2.3 photons per bit for $M = 8$ CFSK. Measured maximal advantage of the receiver in comparison to the SNL is 4.6 dB for $M = 4$ and 0.4 dB for $M = 8$. The observed advantage of the quantum measurement (comparing the measured error rate to the classical SNL with the equal system efficiency) is nearly 8 dB for the $M = 4$ alphabet and 3.5 dB for the $M = 8$ alphabet. The observed advantage of this receiver over classical measurement is greater for CFSK than it is for PSK, owing to the additional optimization flexibility of the CFSK.

We point out that due to the inherent simplicity of the generalized Bondurant receiver, the discriminating module of the receiver (a cyclic counter register) remains the same regardless of

OSA CONTINUUM

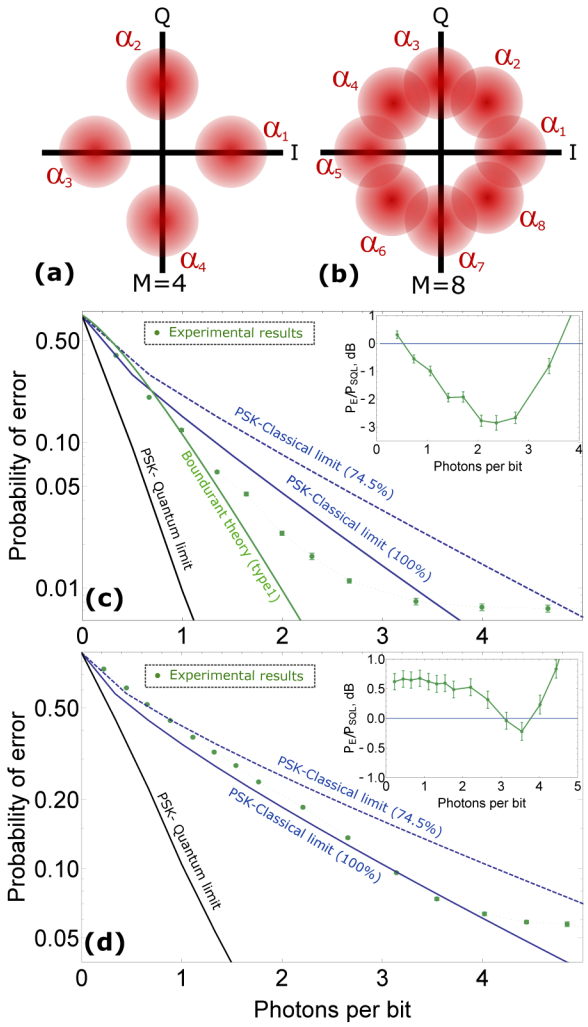

Fig. 2. Constellation diagram of a PSK alphabet with (a) $M = 4$ and (b) $M = 8$. Discrimination error probability for (c) $M = 4$ and (d) $M = 8$ PSK alphabets. To aid comparison between different alphabet lengths, the energy of the input state is represented as photons per bit. Black solid line - HB; green solid line - theoretical performance of the type-1 Bondurant receiver scaled to our system efficiency; blue solid line - unconditional SNL; blue dashed line - SNL scaled to our system efficiency. Inset: the ratio of the observed error probability to the unconditional SNL vs. input state energy.

OSA CONTINUUM

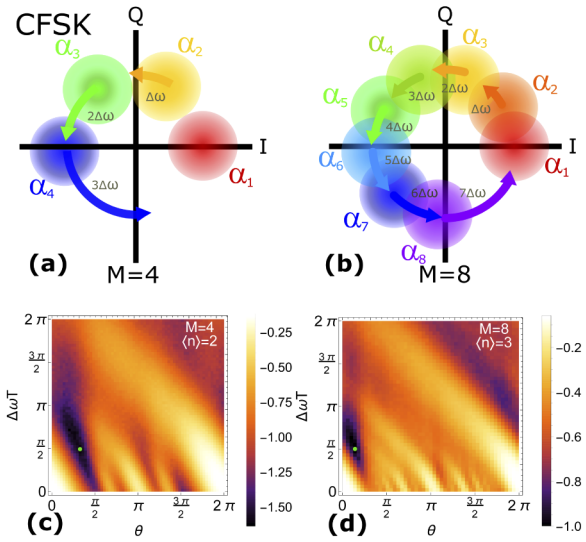

Fig. 3. Constellation diagram of an M-ary CFSK for (a) $M = 4$, (b) $M = 8$. CFSK states revolve around the origin at different rates represented by the length of arrows in the rotating frame of the first state. Optimizing the discrimination error probability using CFSK parameters $\Delta\omega$T and $\Delta\theta$ for (c) $M = 4$ (d) $M = 8$ at the input energy of one photon per bit, see text. The green dot shows the values used in the experiment.

the encoding type. In addition, the energy use of auxiliary computation resources at the receiver required to update a hypothesis is minimal. The experimentally observed sizeable advantage of the cyclic modification of the Bondurant receiver over an ideal classical receiver is obtained in the presence of multiple experimental deficiencies. These deficiencies include non-ideal displacement (i.e. interferometric visibility below unity), dark counts of the detector, inactive time of the detector [33,34], and the delay due to finite speed of sound in AOMs and settling of the DAC. The later delay becomes significant at higher input energies, causing the saturation of discrimination error probability.

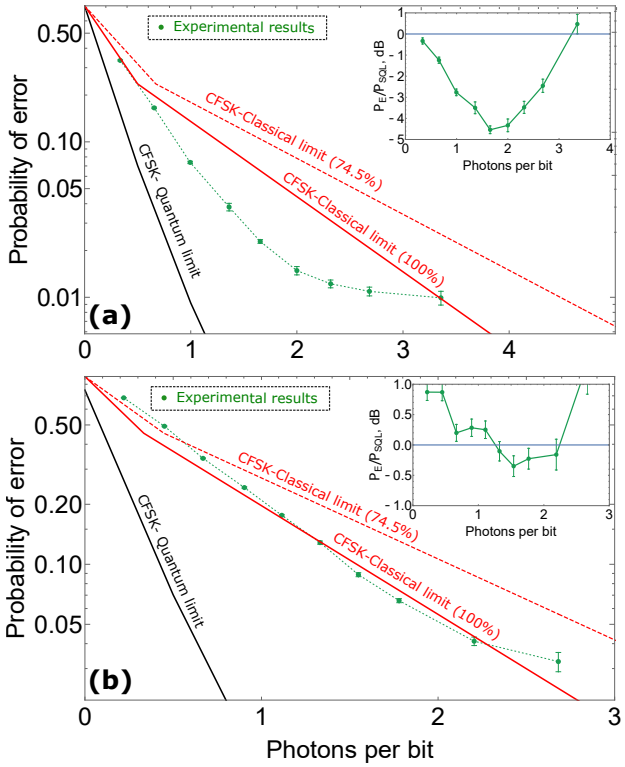

Fig. 4. Discrimination error probability vs. the energy of the input state for (a) M = 4 and (b) M = 8 CFSK. Black solid line - HB; red solid line - unconditional SNL; red dashed line - SNL with matching system efficiency. Inset: the ratio of the observed error probability to the SNL vs. input state energy

4. Conclusion

We have experimentally demonstrated a scalable, versatile cyclic receiver based on the original proposal of Roy S. Boundurant. We experimentally demonstrated the discrimination error rates below the classical limit (SNL) for $M = 4$ and 8 alphabets, and two different modulation methods: PSK and CFSK. Because we used the optimized displacement, the experimentally measured discrimination error rate outperforms the theoretical prediction for type 1 Bondurant's receiver for QPSK at low input energies. In comparing our QPSK results to previous receivers, we show similar advantage over the SNL for the input energies below 2 photons per bit. The discrimination error rate saturation with energy is limited in our implementation by the speed of sound in AOMs. We show that the energy efficiency of the receiver can be further improved with the use of CFSK. The optimal error rate improvement for cyclic receivers requires a different set of CFSK modulation parameters than the optimal parameter set that achieves the lowest error rate with Bayesian displacement receivers, a non-trivial and unexpected result. This surprisingly simple receiver opens practical opportunities to use quantum optical measurement in different settings, and particularly to enhance channel capacity of classical telecommunications with light.

Funding

National Science Foundation (ECCS 1927674).

OSA CONTINUUM

Acknowledgments

Partially supported by the National Science Foundation (ECCS 1927674).

Disclosures

The authors declare no conflicts of interest.

References

1. J. G. Proakis and M. Salehi, *Digital communications*, 5th ed. (McGraw-Hill, 2008).
2. R. Landauer, "Irreversibility and heat generation in the computing process," IBM J. Res. Dev. **5**(3), 183–191 (1961).
3. E. Agrell, M. Karlsson, A. R. Chraplyvy, D. J. Richardson, P. M. Krummrich, P. Winzer, K. Roberts, J. K. Fischer, S. J. Savory, B. J. Eggleton, M. Secondini, F. R. Kschischang, A. Lord, J. Prat, I. Tomkos, J. E. Bowers, S. Srinivasan, M. Brandt-Pearce, and N. Gisin, "Roadmap of optical communications," J. Opt. **18**(6), 063002 (2016).
4. R. J. Cesarone, D. S. Abraham, S. Shambayati, and J. Rush, "Deep-space optical communications," in *2011 International Conference on Space Optical Systems and Applications (ICSOS)*, pp. 410–423 (2011).
5. CISCO, "Cisco visual networking index: Forecast and trends, 2017-2022," https://www.cisco.com/c/en/us/solutions/collateral/service-provider/visual-networking-index-vni/white-paper-c11-741490.html (2019).
6. L. Mandel and E. Wolf, *Optical Coherence and Quantum Optics* (Cambridge University Press, 1995).
7. C. M. Caves, "Quantum-mechanical radiation-pressure fluctuations in an interferometer," Phys. Rev. Lett. **45**(2), 75–79 (1980).
8. C. W. Helstrom, "Quantum detection and estimation theory," J. Stat. Phys. **1**(2), 231–252 (1969).
9. S. J. Dolinar, "An optimum receiver for the binary coherent state quantum channel," Research Laboratory of Electronics, MIT, Technical Report (1973).
10. M. P. da Silva, S. Guha, and Z. Dutton, "Achieving minimum-error discrimination of an arbitrary set of laser-light pulses," Phys. Rev. A **87**(5), 052320 (2013).
11. R. S. Kennedy, "A near-optimum receiver for the binary coherent state quantum channel," Research Laboratory of Electronics, MIT, Technical Report (1972).
12. R. S. Bondurant, "Near-quantum optimum receivers for the phase-quadrature coherent-state channel," Opt. Lett. **18**(22), 1896–1898 (1993).
13. K. Tsujino, D. Fukuda, G. Fujii, S. Inoue, M. Fujiwara, M. Takeoka, and M. Sasaki, "Sub-shot-noise-limit discrimination of on-off keyed coherent signals via a quantum receiver with a superconducting transition edge sensor," Opt. Express **18**(8), 8107–8114 (2010).
14. S. Guha, J. L. Habif, and M. Takeoka, "Approaching helstrom limits to optical pulse-position demodulation using single photon detection and optical feedback," J. Mod. Opt. **58**(3-4), 257–265 (2011).
15. K. Tsujino, D. Fukuda, G. Fujii, S. Inoue, M. Fujiwara, M. Takeoka, and M. Sasaki, "Quantum receiver beyond the standard quantum limit of coherent optical communication," Phys. Rev. Lett. **106**(25), 250503 (2011).
16. K. Kato, M. Osaki, M. Sasaki, and O. Hirota, "Quantum detection and mutual information for qam and psk signals," IEEE Trans. Commun. Technol. **47**(2), 248–254 (1999).
17. F. E. Becerra, J. Fan, G. Baumgartner, S. V. Polyakov, J. Goldhar, J. T. Kosloski, and A. Migdall, "*m*-ary-state phase-shift-keying discrimination below the homodyne limit," Phys. Rev. A **84**(6), 062324 (2011).
18. Y. Zuo, K. Li, and B. Zhu, "16-QAM quantum receiver with hybrid structure outperforming the standard quantum limit," MATEC Web Conf. **61**, 06008 (2016).
19. C. R. Müller and C. Marquardt, "A robust quantum receiver for phase shift keyed signals," New J. Phys. **17**(3), 032003 (2015).
20. F. Becerra, J. Fan, G. Baumgartner, J. Goldhar, J. Kosloski, and A. Migdall, "Experimental demonstration of a receiver beating the standard quantum limit for multiple nonorthogonal state discrimination," Nat. Photonics **7**(2), 147–152 (2013).
21. F. Becerra, J. Fan, and A. Migdall, "Photon number resolution enables quantum receiver for realistic coherent optical communications," Nat. Photonics **9**(1), 48–53 (2015).
22. J. Chen, J. L. Habif, Z. Dutton, R. Lazarus, and S. Guha, "Optical codeword demodulation with error rates below the standard quantum limit using a conditional nulling receiver," Nat. Photonics **6**(6), 374–379 (2012).
23. I. A. Burenkov, O. V. Tikhonova, and S. V. Polyakov, "Quantum receiver for large alphabet communication," Optica **5**(3), 227–232 (2018).
24. M. T. DiMario and F. E. Becerra, "Robust measurement for the discrimination of binary coherent states," Phys. Rev. Lett. **121**(2), 023603 (2018).
25. M. L. Shcherbatenko, M. S. Elezov, G. N. Goltsman, and D. V. Sych, "Sub-shot-noise-limited fiber-optic quantum receiver," Phys. Rev. A **101**(3), 032306 (2020).
26. S. Izumi, J. S. Neergaard-Nielsen, and U. L. Andersen, "Tomography of a feedback measurement with photon detection," Phys. Rev. Lett. **124**(7), 070502 (2020).
27. K. Tsujino, D. Fukuda, G. Fujii, S. Inoue, M. Fujiwara, M. Takeoka, and M. Sasaki, "Quantum receiver beyond the standard quantum limit of coherent optical communication," Phys. Rev. Lett. **106**(25), 250503 (2011).

OSA CONTINUUM

28. S. Izumi, J. S. Neergaard-Nielsen, S. Miki, H. Terai, and U. L. Andersen, "Experimental demonstration of a quantum receiver beating the standard quantum limit at telecom wavelength," Phys. Rev. Appl. **13**(5), 054015 (2020).
29. I. Burenkov, M. Jabir, A. Battou, and S. Polyakov, "Time-resolving quantum measurement enables energy-efficient, large-alphabet communication," PRX Quantum **1**(1), 010308 (2020).
30. A. R. Ferdinand, M. T. DiMario, and F. E. Becerra, "Multi-state discrimination below the quantum noise limit at the single-photon level," npj Quantum Inf. **3**(1), 43 (2017).
31. E. A. Donley, T. P. Heavner, F. Levi, M. O. Tataw, and S. R. Jefferts, "Double-pass acousto-optic modulator system," Rev. Sci. Instrum. **76**(6), 063112 (2005).
32. τ-SPAD, PicoQuant, jitter time of <500 ps, dead time <70 ns, and dark count rate <20 cps. Please note that certain commercial equipment identification does not imply recommendation or endorsement by the National Institute of Standards and Technology, nor does it imply that the materials or equipment identified are necessarily the best available for the purpose.
33. S. V. Polyakov and A. L. Migdall, "High accuracy verification of a correlated-photon-based method for determining photon-counting detection efficiency," Opt. Express **15**(4), 1390–1407 (2007).
34. M. A. Wayne, J. C. Bienfang, and S. V. Polyakov, "Simple autocorrelation method for thoroughly characterizing single-photon detectors," Opt. Express **25**(17), 20352–20362 (2017).

129.6.222.191 {ts '2021-04-16 19:42:07'}